J Mater Sci (2011) 46:3669–3686
DOI 10.1007/s10853-011-5378-y

REVIEW

A review on nano-TiO_2 sol–gel type syntheses and its applications

D. P. Macwan · Pragnesh N. Dave · Shalini Chaturvedi

Received: 28 December 2010 / Accepted: 7 February 2011 / Published online: 16 February 2011

Abstract Nanomaterials, defined as particles ranging from 1 to 100 nm diameter, have become widely utilized because of their unique physicochemical properties. Among those nanoparticles, titanium dioxide (TiO_2) is frequently used in the production of paints, paper, plastics, welding rod-coating material, cosmetics, etc. TiO_2 is the most commonly used semiconductor photocatalyst. Among the different nanomaterials, it is the most studied. Activated by UV-A irradiation, its photocatalytic properties have been utilized in various applications. A wealth of information on TiO_2 photocatalytic in activation of bacteria has been acquired over the last 20 years. Hence, in this review article we have described synthesis methods mainly sol–gel type method like sol–gel method, ultrasonic-assisted sol–gel method, microemulsion method, colloidal synthesis, and also other method are discussed like solvothermal method, thermal plasma process, supersonically expanded plasma jet method, induction plasma torch, reactive plasma processing, plasma electrolytic oxidation, hydrolysis method, thermohydrolysis method, coprecipitation method, citrate–nitrate autocombustion method, etc. Also applications of TiO_2 like medical applications, environmental application, sensor application, photocatalytic applications, and also its health impact for long-term exposure are discussed.

D. P. Macwan
Department of Chemical Engineering, Institute of Nirma University, Ahmedabad, Gujarat 382481, India

P. N. Dave (✉) · S. Chaturvedi
Department of Chemistry, Krantiguru Shyamji Krishna Verma Kachchh University, Mundra Road, Bhuj, Gujarat 370 001, India
e-mail: pragneshdave@gmail.com

Introduction

Titanium dioxide or titania

Titania is a very well-known and well-researched material due to the stability of its chemical structure, biocompatibility, physical, optical, and electrical properties. Its photocatalytic properties have been utilized in various environmental applications to remove contaminants from both water and air [1]. Titania-based photocatalytic systems are used for a variety of applications such as decomposition of unwanted and toxic organic compounds, destruction of pollutants from contaminated water and air and killing of harmful bacteria and cancer cells [2–5]. The unique feature of the photocatalytic process is that it breaks down the pollutants and harmful organic compounds into simple molecules such as carbon dioxide and water [6]. Due to its stability in harsh environments, titanium dioxide (TiO_2) is a ceramic that has the potential to be the material of choice for gas sensors that operate at temperatures above 400 °C [7].

It exists in three mineral forms viz: anatase, rutile, and brookite (Fig. 1) [8]. Anatase type TiO_2 has a crystalline structure that corresponds to the tetragonal system (with dipyramidal habit) and is used mainly as a photocatalyst under UV irradiation. Rutile type TiO_2 also has a tetragonal crystal structure (with prismatic habit). This type of titania is mainly used as white pigment in paint. Brookite type TiO_2 has an orthorhombic crystalline structure. TiO_2, therefore is a versatile material that has applications in various products such as paint pigments, sunscreen lotions, electrochemical electrodes, capacitors, solar cells, and even as a food coloring agent and in toothpastes [9].

In general, TiO_2 is preferred in anatase form because of its high photocatalytic activity, since it has a more negative

conduction band edge potential (higher potential energy of photogenerated electrons), high specific area, non-toxic, photochemically stable and relatively in-expensive. Anatase-TiO_2 for its strong photoinduced redox power was found to be a superior photocatalytic material for purification and disinfection of water and air, as well as remediation of hazardous waste [10].

$$\text{Thermal conductivity of } TiO_2 = 22\ \text{Wm}^{-1}\ \text{k}^{-1}$$
$$\text{Melting point of } TiO_2 = 1,941\ \text{K}$$
$$\text{Boiling point of } TiO_2 = 3,546\ \text{K}$$

Photocatalysis

Photocatalysis may be termed as a photoinduced reaction which is accelerated by the presence of a catalyst. These type of reactions are activated by absorption of a photon with sufficient energy (equals or higher than the band-gap energy of the catalyst) [11]. The absorption leads to a charge separation due to promotion of an electron (e^-) from the valence band of the semiconductor catalyst to the conduction band, thus generating a hole (h^+) in the valence band (the schematic diagram of the process is presented in Fig. 2 [12]. The recombination of the electron and the hole must be prevented as much as possible if a photocatalyzed reaction must be favored (Fig. 2).

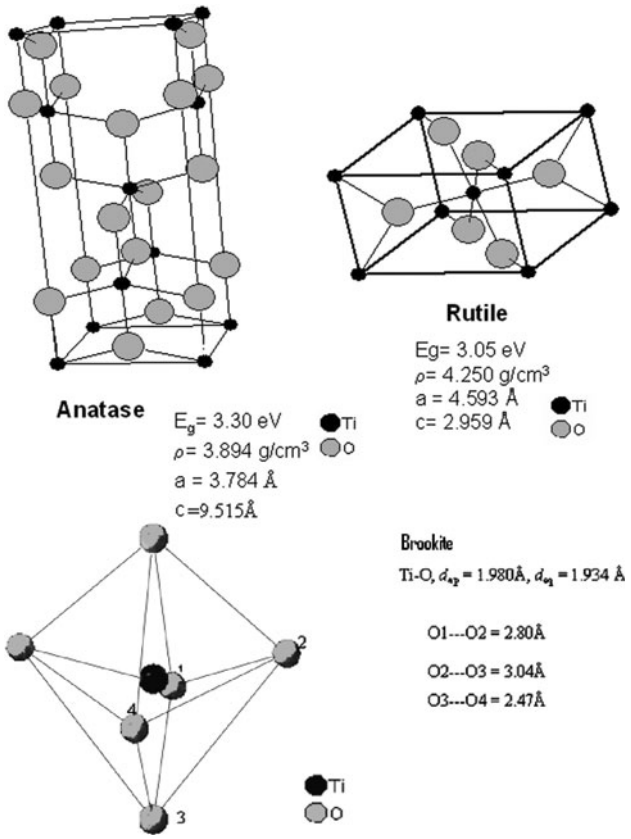

Fig. 1 Different forms of TiO_2

Photocatalytic properties of nano-TiO_2

In recent years, the wide spread presence of chemicals such as heavy metals, herbicides, pesticides, aliphatic and aromatic detergents, arsenic compounds, solvents, degreasing agents, volatile organics, and chlorophenols pose a serious threat to the environment. When such chemicals contaminate water sources, they become really hazardous. For instance, waste waters produced from textile and dyestuff industrial processes contain large quantities of azo dyes. It is estimated that 15% of the total dye is lost during dying process and released in waste waters. Oxidation of these organic pollutants at the surface of TiO_2 catalyst is an important photocatalysis application. Heterogeneous photocatalysis is a process in which a combination of photochemistry and catalysis are operating together. It implies that both light and catalyst are necessary to bring out the chemical reaction. UV light illumination over a semiconductor like TiO_2 produces electrons and holes. The valence band holes are powerful oxidants, while the conduction band electrons are good reductants [13].

What happens on nanoscale

Materials reduced to the nanoscale can suddenly show very different properties compared to what they exhibit on a microscale because of two effects.

Surface effects

1. More % of atoms on surface compared to inner atoms.
2. More surface free energy available: this increased surface area and surface atoms results in the increase of surface energy associated with the particles.
3. Increasing the surface area of a substance generally increases the rate of a chemical reaction.

Volume effects

1. Lower wavelength (higher frequency and higher energy).
2. Blue shift of atoms for optical absorption spectra.
3. *Magnetism*: when the particle is smaller than the magnetic domain in a magnetic material.
4. In a free electron model average energy spacing increases as the number of atoms reduce. This enhances the catalytic properties of nanoparticles.

Semiconductor materials

Semiconductor materials are materials whose valence band and conduction band are separated by an energy gap or band

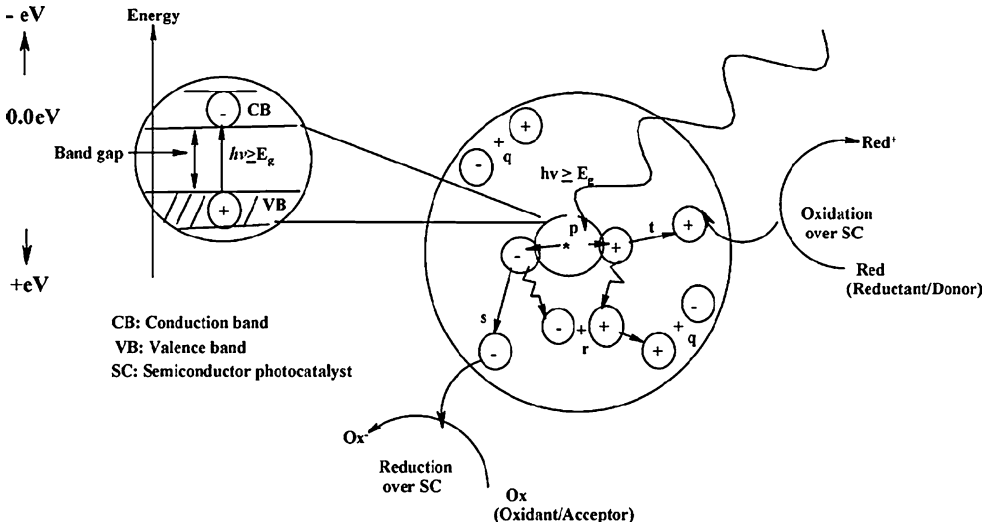

Fig. 2 Schematic diagram of photocatalytic process initiated by photon acting on the semiconductor

gap. When a semiconductor molecule absorbs photons with energy equal or greater than its band gap, electrons in the valence band can be excited and jump up into the conduction band, and thus charge carriers are generated. In order to have a photocatalyzed reaction, the electron–hole recombination, subsequent to the initial charge separation, must be prevented as much as possible [14]. Among all these semiconductors, the most widely used semiconductor catalyst in photoinduced processes is titanium dioxide (TiO_2). Though TiO_2 has the disadvantage of not being activated by visible light, but by ultraviolet (UV) light, it is advantageous over the others in that it is chemically and biologically inert, photocatalytically stable, relatively easy to produce and to use, able to efficiently catalyze reactions, cheap and without risks to environment or humans [11]. The performance of TiO_2 for certain technical application is dominantly influenced by its crystallite size, surface area, phase structure, and impurity (dopant) type and concentration [15]. Recently, it was demonstrated that doping TiO_2 with silver greatly improved photocatalytic inactivation of bacteria [16, 17] and viruses. Visible light absorption by silver surface plasmons is thought to induce electron transfer to TiO_2 resulting in charge separation and thus activation by visible light. Band gaps of both ZnO and TiO_2 have been modified by nonmetals and transition metals doping. Each dopant has a unique effect on the optical properties and photocatalytic activity of these semiconductor oxides [18]. TiO_2 is reported to absorb visible light via artificially created oxygen vacancies in its crystal structure [19, 20]. Oxygen vacancies are generated in TiO_2 by plasma treatment through radio-frequency discharge [19]. Although oxygen vacancies can activate TiO_2 under visible light they can also promote electron–hole recombination process.

Methods for synthesis

Many methods have been reported for the production of TiO_2 nanopowders such as chemical solution decomposition (CSD) [21], chemical vapor decomposition [22–24], two-step wet chemical method [25], sol–gel [26–60], ultrasonic irradiation [61, 62], ethanol thermal and hydrothermal [63–66].

The most widely used TiO_2 in photocatalysis is commercial Degussa P25 produced by flame hydrolysis of $TiCl_4$ at temperatures greater than 1,200 °C in the presence of hydrogen and oxygen. Recent literature [26–60] revealed that sol–gel is the most commonly used method for the preparation of photocatalysts, whether only TiO_2 or doped TiO_2. The advantage of these methods (wet chemical methods, which include sol–gel) is that they facilitate the synthesis of nanometer sized crystallized TiO_2 powder of high purity at relatively low temperature [61]. Modified sol–gel method has also been used [67, 68], ultrasonic-assisted sol–gel method [69], aerogel method [70], method similar to sol–gel [71], sol–gel and photoreductive decomposition [72], precipitation [73, 74], two-step wet chemical method [25], and extremely low temperature precipitation [75]. One commonly encountered problem is that these methods may generate amorphous or low crystallinity products, which necessitates a subsequent annealing for crystallization or further crystallization. Such a thermal annealing, however, may cause hard aggregation and even inter-particle sintering [15]. Plasma-assisted processes exhibit good crystallinity [76, 77]. Recently, a surge in interest was observed to study plasma-assisted nanocrystalline titania synthesis processes by optical emission spectroscopy (OES), for better understanding of the detailed chemistry involved. Oxidation of titanium was

extensively studied in laser-ablated plasmas [78–80], in magnetron sputtering [81], transferred arcs [82], and microwave discharge plasma systems [83, 84].

Distinct advantages of plasma processing, in terms of powder synthesis, reside in that the resultant particles are of high purity and are largely dispersed [15]. Flame aerosol processing and plasma processing using liquid precursors have also been used [15, 85, 86]. The main disadvantage of the solution precursor plasma route is that it consumes large energy for vaporization of the solvent [6].

Brief description of methods for synthesis of nano-TiO_2

Sol–gel preparation

The nanocrystalline titanium dioxide sol–gel formulations were prepared by hydrolysis and condensation reaction of 5% titanium tetra-isopropoxide in acidic aqueous containing 5% acetic acid and 1.4% hydrochloric acid. The solutions were heated at 60 °C under vigorous stirring for 2 and 16 h. The 2 and 16 h formulations are termed T2 and T16, respectively.

Results of X-ray diffraction (XRD) suggest that particle size of the sols varied with the preparation time. In T2, the main peak of particle size decreased from 40 to 25 nm. The particle size distribution of T16 ranged from 15 to 75 nm, whereas that of T2 was narrower and ranged from 10 to 50 nm. XRD also suggests that formation of anatase phase was observed with high crystallinity and sharp anatase peaks. From selected area electron diffraction (SAED) lattice spacing for anatase crystallites can be observed in the SAED inset. Finally, T2 sol demonstrated a more transparent formulation with smaller particles size distribution [87].

How dopants could be helpful with sol–gel preparation?

It is reported that the addition of Zn^{2+} could enhance the photoactivity of TiO_2 significantly; however, these titanium dioxides completely transformed to the rutile structure at about 500 °C. They also found that by sulfating the Zn-doped TiO_2, the *anatase-to-rutile phase transformation* can be restrained and the sulfated Zn-doped TiO_2 at 700 °C had the major crystalline phase of anatase-TiO_2. Phosphoric acid solution added to the TiO_2 suspension, obtained by sol–gel synthesis, to prepare phosphate-modified TiO_2 (P-TiO_2). It is reported that the presence of phosphate shifted the anatase-to-rutile phase transformation to higher temperatures. The specific surface area and semiconductor band-gap energy of the P-TiO_2 increased with the phosphate content but decreased with calcination temperature. For application like, photooxidation of phenol, they concluded that P-TiO_2 with phosphate content <3 wt% was more active than pure TiO_2 [88].

Preparation

TiO_2 nanoparticles, with zinc and/or phosphorus dopants, were prepared by a sol–gel method. 50 mL of the alcoholic solution containing 0.06 mol tetra ethyl orthotitanite [TEOT; $Ti(OC_2H_5)_4$; 95% purity] were mixed with 500 mL of the aqueous solution of zinc nitrate [$Zn(NO_3)_2{\cdot}6H_2O$; 99% purity] and phosphoric acid (H_3PO_4; 98% purity). The total number of moles of zinc nitrate and phosphoric acid in the aqueous solution was 5% of the number of moles of TEOT used, and the molar ratio of phosphoric acid and zinc nitrate was varied (i.e., $[H_3PO_4]/[Zn(NO_3)_2] = 0$–3). The mixture was then refluxed at 90 °C for 4 h, followed by cooling of the resultant suspension to room temperature. Then after centrifugal filtration the collected solids were dried at 90 °C for 24 h and dried solids were then calcined in air at different temperatures, ranging 400–1,000 °C for 2 h, respectively.

P/Zn–TiO_2 nanoparticles, with a molar ratio $[P + Zn]/[TiO_2] = 0.05$, were synthesized using a sol–gel method. The effects of $[H_3PO_4]/[Zn(NO_3)_2]$ molar ratios and calcinations temperatures on phase transformation and photocatalytic ability of the P/Zn–TiO_2 were examined.

P/Zn–TiO_2 nanoparticles prepared using $[H_3PO_4]/[Zn(NO_3)_2] \geq 2$ not only can totally stabilize anatase-TiO_2 at 800 °C, but also exhibit superior photocatalytic abilities. These P/Zn–TiO_2 particles were prepared at 600–800 °C can decompose ≥96 mol% of the MB after 30 min of the UV irradiation and ≥80 mol% of the MB after 60 min of the white light irradiation, which is much better than those of the P25 particles [10].

Ultrasonic-assisted sol–gel method

For this method, ultrasonic waves consisting of compression and rare fraction cycles produce cavitation bubbles in liquid solution. After several compression cycles, the cavitation bubbles collapse violently and adiabatically at extremely high temperatures of up to 5,000 °C and pressures of about 500 atm [89, 90]. Thus, such extreme temperatures and pressures within a small reactor can induce many changes in the morphology of TiO_2 nanoparticles during preparation.

In the case of the ultrasonic-assisted synthesis of TiO_2, such operating variables as the ultrasonic power density, reactor size, stirring effect, and mode of application for the ultrasonic waves, etc., may have a strong influence on the properties of mesoporous TiO_2 photocatalysts, apart from the chemical influence on their morphology. Thus, with the ultrasonic-assisted sol–gel method, the control of many important parameters such as the particle size, surface area, pore volume, pore size, anatase and rutile phase ratio, and crystallinity is possible.

Preparation of nanosize-TiO_2 particles

TiO_2 photocatalysts were synthesized by sol–gel and ultrasonic-assisted sol–gel methods, in which titanium tetraisopropoxide (TTIP) was used as the precursor [91]. The ratio of water and TTIP was 175 for sol–gel and 35 for the ultrasonic-assisted methods. In this study, two different ultrasonic sources were used and compared. One is the Branson, commonly used for cleaning purposes in laboratories and the other is the Sonics Vibracell. The Vibracell is mostly used for the ultrasonic-assisted degradation of organic pollutants as well as the synthesis of nanoparticles. The tip-US type, i.e., a probe type ultrasonicator and reactor setup have been reported [92, 93]. The ultrasonic power of both ultrasonicators was determined by the Calorimetry method [94].

The ultrasonic power of the bath-type ultrasonicator is 157 W and of the tip-type is 30 W at 40% amplitude. The frequency of the tip-type and bath-type ultrasonicators was 20 and 40 kHz, respectively. The TiO_2 catalyst prepared by the Branson instrument was denoted as the bath-US and the Vibracell device was denoted as the tip-US. With the Vibracell, a tip horn was used to produce the ultrasonic irradiation inside the reactor and sol–gel mixture, whereas with the bath-US, ultrasonic irradiation was applied from outside the reactor. The TiO_2 photocatalysts were prepared by these bath-US and tip-US methods, in which hydrolysis of titanium isopropoxide took place under ultrasonic irradiation at 1 h in a continuous mode.

For the tip-US method, the temperature of the double-walled reactor was maintained at around 20 °C using a cooling device. After preparation of TiO_2 by these three different methods, the catalysts were kept for 20 h for slow hydrolysis at room temperature, dried at ambient temperatures for 12 h and calcined at 500 °C in a furnace under the continuous flow of air for 3 h [95].

Microemulsion method

Sol–gel method need of costly organic solvents is a disadvantage.

Preparation

Polymeric surfactant poly(dimethyl aminoethyl methacrylate-block-1H,1H,2H,2H-perfluorooctylmethacrylate) $PDMAEMA_{2k}$-b-$PFOMA_{10k}$ was synthesized by sequential addition of DMEMA and FOMA via group transfer polymerization. The cell was immersed in a water bath and the temperature of the cell was controlled by the water bath. Pressure was controlled using a high pressure generator. An external magnetic stirrer was used with a PTFE-coated magnetic bar. The W/C microemulsions were prepared by adding the PDMAEMA-b-PFOMA surfactant to the cell, followed by the addition of water to achieve the desired water-to-surfactant ratio (W0) and then the cell was loaded with carbon dioxide at the experimental temperature, and the pressure was raised up to 3,000 psi with continuous stirring for 30 min. Finally, an adequate amount of TTIP was added and then the pressure of the cell was controlled to 4,000 psi for 30 min to prepare titanium hydroxide. The prepared nanosized particles were washed by ethanol and dried at 105 °C for 1 day and then calcined at 500 °C for 3 h.

The crystallite size can be controlled by the water-to-surfactant mole ratio (W0), which influences the hydrolysis rate, droplet size, and intermicellar interactions. The XRD pattern of the particle dried at 105 °C without calcinations indicate amorphous and the particles calcined at 500 °C were identified as a nanocrystalline anatase regardless of W0 ratio. The crystallite size of particle increases from 8 to 18 nm and the photocatalytic activity decreases with an increase of W0 ratio. The TiO_2 particles prepared by the microemulsion method showed higher activity than the bulk TiO_2 [96].

TiO_2 colloidal synthesis

Titanium isopropoxide (97%) was added drop wise to 0.1 M nitric acid solution (125–750 mL, respectively) under vigorous stirring. White slurry formed and this slurry was heated to 80 °C, stirred for 3 h to achieve peptization (i.e., destruction of the agglomerates and re-dispersion into primary particles). The solution was then filtered in a funnel provided with glass frit to remove non-peptized agglomerates. Hydrothermal treatment of the solution in an autoclave was carried out for 12 h at 250 °C. Sedimentation occurs during the autoclaving, and the particles are re-dispersed by two consecutive sonications. Then, the colloidal suspension is introduced in a rotary evaporator set at 35 °C, 3 MPa and brought to a final TiO_2 concentration of 11 wt%. Nanocrystalline anatase TiO_2 with small particles size distribution of 8–18 nm was synthesized [97].

Solvothermal method

Solvothermal method is an alternative route for direct (one-step) synthesis of pure anatase nano-TiO_2. Quenching process has been applied as a post-synthesis treatment for enhancement of photocatalytic activity of nano-TiO_2 synthesized by solvothermal method. Quenching is defined as the mechanism of "rapid cooling" of material [98].

Preparation

Titanium (IV) *n*-butoxide (purity 97%) was used as the starting material. Approximately, 25 g of titanium *n*-butoxide was suspended in 100 mL of toluene, in a test tube, which was then placed in a 300 mL autoclave. The same solvent was filled in the gap between the test tube and the autoclave wall. The autoclave was purged completely by nitrogen after that it was heated up to the desired temperature at 573 K with the rate of 2.5 K/min. The temperature of the autoclave was held constant at 573 K for 2 h and then cooled down to room temperature. The obtained TiO_2 was washed by methanol for several times and finally dried in air.

Quenching treatment

Prior to quenching, the synthesized TiO_2 was dried in air atmosphere at 573 K with a heating rate of 10 K/min for 1 h and then it was taken out and immediately quenched in various quenching media. In this study, both liquid-phase and gas-phase media were used. For quenching in liquid-phase media, liquid nitrogen at 77 K (sample A), water at room temperature and 373 K (samples B and C), and hydrogen peroxide (30% wt) at room temperature and 373 K (samples D and E) were selected. For quenching in gas-phase media, air at room temperature and 77 K (samples F and G) were used. After the samples were quenched in selected media for 30 min, all samples were dried in air at room temperature and stored in desiccators.

Result of XRD shows 10–13 nm size of particles. High-resolution transmission electron microscopy (HRTEM) suggests that crystalline particles are formed with primarily spheroidal shape with the size around 8–15 nm. Quenching process especially the use of low temperature medium can create a thermal shock effect that as a consequence resulting in more surface Ti^{3+} defects on the TiO_2 sample and hence higher photocatalytic activity [99]

Solvothermal method for synthesis of nano-Bi/TiO_2

Preparation

The reagents used for the preparation of sol-mixture were titanium tetra-isopropoxide or TTIP (99.95%) and bismuth (III) chloride (99.99%), which were used as Ti and Bi precursors. Metal precursors were mixed with ethyl alcohol (99%) in an autoclave heated at 200 °C for 10 h at a rate of 10 °C/min. The molar ratios of Bi:Ti precursors in gel mixtures were kept to molar ratio of 1:10. During thermal treatment, Ti and Bi were hydrolyzed by the OH group in solvent and then the crystallized nano-sized Bi/TiO_2 occurred. The resulting powder was washed with distilled water until pH 7 and then dried. Finally, to remove impurities, which remained carbon or chloride ions on the surface of the powders, these samples were thermal treated at 500 °C for 3 h.

Unlike in the sol–gel method, the crystallized TiO_2 nucleus occurred in thermal treatment in high temperature and pressure, and then grew up to primary particle through homo-coagulation. At this point, the excess solvents partially suppressed more crystal growth; as a result, the particle size became finer than that in the sol–gel method. Finally, the TiO_2 anatase particles were attained without the calcinations step [100].

Result of FESEM says that both catalysts TiO_2 and Bi/TiO_2 were shown to consist of relatively uniform and spherical particles with sizes of about 25 nm. XRD and Raman spectroscopy confirm that the Bi ions were well substituted to Ti sites. The surface area was large (310 m^2/g) as compared with that of pure TiO_2 (140 m^2/g). Bi/TiO_2 (10.0 mol%) adsorbed smaller water amount than pure TiO_2 [101] (Fig. 3).

Preparation of TiO_2 aqueous dispersion

Degussa P-25 TiO_2 powder was employed without further treatment. It is said that Degussa P-25 TiO_2 powder is approximately spherical and nonporous with >99.5% purity and contained about 80% of anatase and 20% of rutile and the average particle size of the TiO_2 particles was 30 nm [102]. All other chemicals were of reagent grade. TiO_2 aqueous dispersion was prepared by mixing 1.5 g of Degussa P-25 TiO_2 powder and the appropriate amounts of deionized water in an ultrasonic mixer. After 5 h of ultrasonic mixing, 0.125 g of polyglycol was added into aqueous dispersion and mixed under continuous magnetic stirring for 30 min. The TiO_2 aqueous dispersion was prepared containing 3% by weight of Degussa P-25 TiO_2 and 0.25% by weight of polyglycol. The average particle

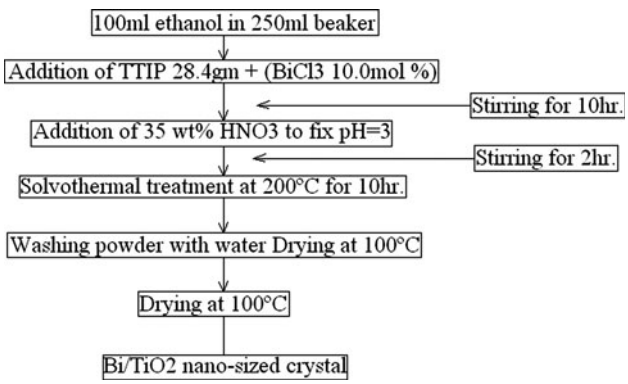

Fig. 3 Preparation of TiO_2 and 10.0 mol% Bi/TiO_2 nm particles by solvothermal method

size was measured in TiO_2 aqueous dispersion to be 0.212 mm [103].

Thermal plasma process

Although the sol–gel method is considered as a suitable method to synthesize ultrafine particle, this method needs a large quantity of solution, longer processing time and heat treatment for crystallization because amorphous TiO_2 has a little photocatalytic activity. The particle agglomeration and growth is unavoidable during post-heat treatment. In sputtering method, high quality TiO_2 can be produced but it costs much.

However, the thermal plasma process has unique characteristics for preparing nanopowders. The high temperature and rapid cooling involved the plasma processing gave the short processing time. The thermal plasma process is used to synthesize nano-sized TiO_2 powder.

Preparation

Nano-sized titanium dioxide was synthesized from titanium tetrachloride ($TiCl_4$, 99.9%) in a thermal plasma reactor. The plasma torch consists of tungsten cathode and copper anode, and the plasma was generated by Ar gas. $TiCl_4$ was injected into the plasma region through the injection block by Ar carrier gas. Aluminum chloride ($AlCl_3$, 99%) in methanol solution was added to the plasma reactor through the injection block by using metering pump. The synthesized powders were collected mainly at the reactor wall by using round shaped spoons. The exhaust gases passed through a scrubber to remove chlorine compounds.

Results of XRD suggest that the noticeable change could not be found in the phase by an introduction of Al dopant. Scanning electron microscopy (SEM) says that with the increase of Al dopant, the size of the particles decreased. Transmission electron microscopy (TEM) shows the range of size is from 10 to 50 nm in the Al-doped TiO_2. Optical property shows that band edge of the powders shifted from UV region to visible region [104].

Thermal plasma method using liquid precursor

Preparation

Water-cooled induction plasma torch is used for powder synthesis, a liquid precursor is delivered by a peristaltic pump into the center of the Ar/O_2 plasma plum through an atomization probe. Feeding rate of the precursor is controlled at $\sim$4 mL/min. The liquid precursor is made by adding certain amounts of diethanolamine ($HN(OC_2H_5)_2$) to 0.125 mol of titanium butoxide ($Ti(OC_4H_9)_4$) under water cooling and magnetic stirring. The Ar/O_2 thermal plasma is generated by mixing O_2 in the Ar sheath (casing). The TiO_2 nanoparticles formed via instantaneous oxidation of the atomized liquid droplets by Ar/O_2 thermal plasma mainly deposit on the filter and the inner walls of the reactor.

Product powder mainly contains TiO_2 and is free from titanium sub-oxide impurities, such as Ti_2O_3, Ti_3O_5, Ti_4O_7 and so on and is mixture of the anatase and rutile polymorphs. The anatase content falls in a narrow range of $\sim$71–78 wt%, the crystallite size of anatase varies between $\sim$33 and 40 nm, while that of rutile between $\sim$37 and 43 nm. It is known that the metastable anatase phase transforms to thermodynamically stable rutile in the temperature range $\sim$400–1000 °C depending upon a variety of factors mainly including crystallite size, impurity type and concentration, and atmosphere. The formation of anatase as the major phase in this work, despite the high processing temperature, is owing to the superfast quenching effect of the thermal plasma. The CO gas released via oxidation of the organic precursor has appreciable effects on the phase constituent. The majority of the resultant TiO_2 particles are nanosized ($<\sim$50 nm) [15].

Supersonically expanded plasma jet

It is reported that use of a supersonically expanded plasma jet for controlled synthesis of nanostructured titania, by reacting titanium chloride with oxygen. OES techniques have been used to study the plasma chemistry primarily concentrating on the hot injection zone just beyond the anode, where most of the reactions occur. Spectroscopic techniques have been used for diagnostics of the plasma, as well as for systematic identification of the chemical species taking part in the reactions. Although this particular chemical route is the preferred one for commercial production of titania material in huge amount, the process as a whole is not yet properly understood and remains to be optimized.

Preparation

The segmented plasma torch used here consists of a thoriated tungsten cathode, a stack of insulated, interspaced copper rings and a copper anode, all of which are intensely water cooled. The anode is connected to an injection section (15 mm diameter, 25 mm long) followed by a 50 mm long converging nozzle (inlet diameter of 10 mm and outlet diameter of 5 mm). A tubular furnace is used to evaporate the metal chlorides and inject into the injection section.

Because of a high pressure difference maintained between the injection section and the other end of the

nozzle, the plasma beam accelerates through the converging nozzle and expands supersonically into the low-pressure sample collection chamber. Titania is formed by reacting titanium chloride vapor and oxygen gas in the plasma.

$$TiCl_4 + O_2 \rightarrow TiO_2 + 2Cl_2$$

They have demonstrated synthesis of nanocrystalline, non-agglomerated titanium dioxide particles in a supersonically expanded plasma jet-assisted process, with control over average size of the particles and phase combination. The average particle size increases with the precursor concentration, which may be important for upgrading the technique for commercial production [105].

Induction plasma torch

Plasma, as a high-energy rapid-heating power source, has already been applied to produce TiO_2 powders and thin films. Thin films of TiO_2 were prepared by a plasma spray of fine TiO_2 powders under $Ar–O_2$ thermal plasma, and by plasma implantation of metal Ti [106–110]. Synthesis of TiO_2 powders by plasma was conducted by vapor decomposition and/or oxidation of $TiCl_4$ or other Si-containing precursors. The powder or film produced by such process is usually agglomerated irregularly shaped fine particles in nanosize scale, which are either amorphous or poorly crystallized.

Preparation

Oxidation of TiC micron powders was conducted in an aerosol reactor equipped with an induction plasma torch. The starting TiC powders were a commercial product with a mean diameter of 28 mm. In the oxidation treatment, the TiC powders were injected from the top of the plasma torch into the center of the plasma region by a powder feeder using argon carrier. High purity oxygen (99.99%) was mixed with argon and was injected in two ways: (i) injected as plasma sheath gases; and (ii) injected at the tail portion of the plasma flume. Oxidized products were collected from the reaction chamber.

Results of SEM shows that fine particles in nanosize scale (30–50 nm) were synthesised. XRD suggests that product particles consist of both anatase and rutile, with anatase as the richer component. The amount of the nanosize particles increases with the oxygen input. This process can produce well-defined micron spheres of TiO_2 with a high degree of crystallinity by a one-step process. TiO_2–TiC composite particles with the unique core–shell structure can also be produced by this novel process through controlling oxidation of TiC by using a lower oxygen input in the plasma sheath gases [111].

Reactive plasma processing

A novel method involving "in-flight" oxidation of TiH_2 in thermal plasma jet has been developed for bulk synthesis of nanocrystalline titania [112]. Reactive plasma processing (RPP)is a novel technique that takes advantage of the high temperature and high enthalpy of the thermal plasma jet to effect "in-flight" chemical reactions in the presence of a reactive gas to synthesize nano-sized powder so advanced ceramics, novel coatings and convert mineral sand industrial wastes to value-added materials. The major advantages of the RPP technique include versatility, short processing time, large throughput; adaptability to process thin films and coatings. Also, the process can be customized to synthesize any desired product. The technique is ideally suited for large-scale production.

Reactive plasma synthesis of nano-sized TiO_2 powder

The main components of the plasma reactor include 40 kW DC arc plasma torch, water-cooled reactor segment, product collection facility, DC power supply, water cooling system, and exhaust gas. The DC arc plasma torch is mounted on the reactor, which is a double-walled stainless steel cylindrical vessel 300 mm in diameter and 600 mm in length. The torch electrodes and the reactor are cooled by water. The powder is injected into the plasma jet through aside port provided at the anode of the plasma torch. There is provision to inject oxygen or any desired reactive gas downstream the plasma jet, 10 mm from the nozzle, by means of a gas injector ring fitted on the torch head section. A mixture of argon and nitrogen was used as the plasma gas. The powder feed rate and carrier gas flow rate were monitored and controlled. The experimental run consisted in establishing a stable arc between the electrodes. The plasma gas, introduced in the inter-electrode region, extracts the arc energy and issues out of the anode nozzle as a high temperature, high velocity jet. Desired power level was maintained by controlling the flow rates of the plasma gases and arc current. TiH_2 powder, 99.8% pure was used as the precursor material. TiH_2 powder (38–53 mm size) was injected into the plasma jet by using argon as the carrier gas. Oxygen gas was introduced 10 mm downstream of the exit of the plasma torch. TiH_2 dissociates to form Ti particles and hydrogen gas in the plasma jet that are subsequently converted to TiO_2 and water vapor, which escapes along with the exhaust gas stream. Titanium oxide formed collects as nano-sized dust on the walls of the reactor, collection chamber and flanges. The nano-sized powder of TiO_2 generated by this method is referred to as A1. The plasma reactor was run for 5 min and the total amount of TiH_2 injected into the plasma was 25 g. In order to see the effect of post-treatment on the

photocatalytic properties of RPP powder, a fraction of sample A1 was heated at 500 °C in flowing Ar–8% H_2 gas for 3 h and is called sample A2.

The total weight of TiO_2 collected from different sections of the plasma reactor was found to be 39.45 g (closely matches theoretical value). Complete conversion of TiH_2 to TiO_2 should yield 39.96 g of titanium dioxide. The difference between the weight of TiO_2 collected and the theoretical yield is within experimental error, suggesting complete conversion of the feed material to TiO_2. The content of anatase phase in the processed powder was found to be about 65%. Results of XRD studies indicated that the thermal treatment did not affect the phase composition of A1. Raman spectroscopy suggests that the characteristic bands due to the anatase phase are more intense than those of the rutile phase for the samples A1 and A2 in agreement with the results of XRD. Diffuse reflection spectroscopy shows that the absorption edge of plasma-synthesized TiO_2 nanopowders for samples A1 and A2 appeared at about 420 nm. Since samples A1 and A2 absorb light over a wider range of wavelength and utilize more light energy, it follows that they have higher photocatalytic activity under sunlight radiation. FESEM shows powder (A1 and A2) consists of nano-sized particles with spherical or near-spherical morphology. The particle size is seen to be distributed in the range of 10–50 nm. It is also seen that more than 60% of the particles are distributed in the 20–30 nm range. Evidence for the formation of Ti^{3+} centers and hydroxyl groups on the surface of the powder could be obtained by FTIR and XPS results, which were further corroborated by improved photocatalytic performance [6].

Plasma electrolytic oxidation

Hydroxyapatite ($Ca_{10}(PO_4)_6(OH)_2$, HA) plasma electrolytic oxidation (PEO) is a relatively convenient and effective technique to introduce Ca and P into porous TiO_2 coatings on titanium and its alloys.

Preparation

In the PEO process, Ti_6Al_4V plates (10 × 10 × 1.5 mm) were used as anodes, and stainless steel plates were used as cathodes in an electrolytic bath. The Ti_6Al_4V plates were ground with abrasive papers, ultrasonically washed with acetone and deionized water, then dried at 40 °C. An electrolyte was prepared by dissolving $Ca(CH_3COO)_2{\cdot}H_2O$ (6.3 g/L), $Ca(H_2PO_4)_2{\cdot}H_2O$ (13.2 g/L), EDTA·2Na (15 g/L), and NaOH (15 g/L) into deionized water with addition of nano-HA powder with an average particle size of 50 nm (16 g/L). The applied voltage, frequency, duty cycle, and oxidizing time were 300 V, 600 Hz, 8.0%, and 5 min, respectively. The temperature of the electrolyte was kept at 40 °C by a cooling system. After PEO treatment, each sample was treated in 10 mL NaOH aqueous solution with concentration of 5 mol/L at 60 °C for 24 h, and then gently washed with deionized water and dried at 25 °C (Table 1).

XRD result suggesting an amorphous phase produced by the chemical treatment of the PEO coating. SEM: the PEO coating exhibits a porous surface where the micropores with 3 mm in diameter are distributed uniformly. At a higher magnification it can be seen that the surface of the PEO coating is rough. After chemical etching, the surface of the PEO coating was modified and the size of the micropores decreased to 0.5–1 mm.

Moreover, the CT-PEO coating shows a honeycombed structure composed of numerous nano-flakes (with 100 nm in thickness) and pores (with 100–200 nm in size) around the submicron pores. The addition of nano-HA in the electrolyte has no obvious influence on the apatite-forming ability of the CT-PEO coating [113].

Hydrolysis method

The powder used in this work was synthesized through controlled hydrolysis of titanium butoxide in an ethanol aqueous solution [114]. The morphology of the powder was spherical or ellipsoidal with a size range of 50–100 nm in diameter and the powder was in an amorphous phase state.

XRD analysis of TiO_2 films shows of the three TiO_2 films, it can be seen that, Film (I) was mainly composed of anatase and rutile phases. The diffraction intensity of anatase phase is higher than that of rutile phase and also trace amounts of TiO_2-x was observed [115]. Film (II) was also composed of anatase and rutile phases with a trace of the TiO_2-x phase. The diffraction intensities of rutile and anatase phase were similar, and that of TiO_2-x phase increased. Film (III) was composed mainly of rutile phase with a small amount of anatase and TiO_2-x phases and it can be concluded that the content of anatase phase decreased and that of rutile phase increased from Film

Table 1 Sample labels and treatment condition

Sample	Treatment condition Plasma electrolytic oxidation	Chemical treatment
nPEO	√[a]	–
PEO	√[b]	–
CT-nPEO	√[a]	√
CT-PEO	√[b]	√

"√" With treatment, "–" without treatment

[a] The oxidized coating formed in an electrolyte without addition of HA

[b] The oxidized coating formed in an electrolyte with addition of HA

(I) to Film (II) and Film (III). For morphologies of TiO_2-x Films, SEM micrographs of titania films shows that all three films can be seen and porous nanostructured morphologies. However, the flatness of the films was different. From Film (I) to Film (II) and Film (III), the surface of the films got smoother, the porosity got less, and the pore distribution got more even. TEM micrographs of the three TiO_2 films shows that the three films were composed of nanosized particles and the particles with a size range of 50–100 nm [116].

Thermohydrolysis

Preparation

The anatase particles were obtained through the thermohydrolysis at 95 °C of an aqueous solution of $TiCl_4$ in the presence of glutamic acid, A 250 mL solution of Ti^{4+} (0.082 mol L^{-1}) was prepared, and glutamic acid (0.0082 mol L^{-1}) was introduced as powder under vigorous stirring. The pH of the solution was adjusted to 4 with sodium hydroxide. A white precipitate immediately appeared and the suspension was aged for 48 h in a stove at 95 °C without stirring. The procedure was successfully scaled up from 250 mL to 3.5 L, and the solids were collected by filtration of the colloidal suspension. The particles were flocculated, in order to facilitate the filtration, by increasing the pH up to 6 (close to the isoelectric point) [117] by addition of NaOH and then washed several times with deionized water. Powders were finally dried under air at 100 °C. XRD confirms raw material used was pure phase anatase nanoparticles [118].

Coprecipitation

Preparation

The nanocomposite oxide containing Al_2O_3, ZrO_2, and TiO_2 was prepared by conventional coprecipitation. $Al(NO_3)_3 \cdot 9H_2O$, $ZrO(NO_3)_2 \cdot 2H_2O$, and $TiCl_4$ were dissolved in ion-exchanged water, and then an ammonia solution was added for coprecipitation. The obtained product was dried at 673 K for 5 h and calcined at 1,073 K for 5 h in air.

This result suggests that using the nanocomposite of Al_2O_3 and ZrO_2–TiO_2 as a support is a better method for a NOx storage–reduction catalyst then physically mixed oxide [119] (Fig. 4).

Citrate–nitrate autocombustion method

To obtain optimum and reproducible nano-sized materials, a citrate–nitrate autocombustion method was used which is a modified Pechini method [120]. The Pechini process is

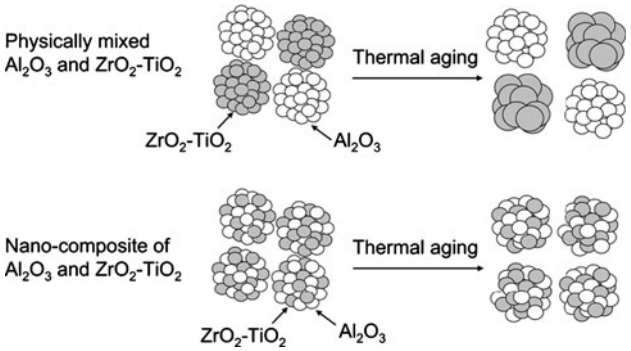

Fig. 4 Concept chart of the nanocomposite of Al_2O_3 and ZrO_2–TiO_2

one of the many sol–gel techniques available, in which a chelated complex is formed between the mixed cations and carboxylic acid groups such as citric acid. This way the cations get uniformly distributed throughout the gel structure. On heating, this chelated polymer complex breaks down, and subsequently the cations are oxidized to form crystallites of metal oxides. It is reported that this method can be used to make pure and doped TiO_2 nanopowder which show good sensitivity toward CO [121].

Preparation

All nanopowder was synthesized using commercial TiO_2 powder. 50 g of commercial TiO_2 powder was kept for 1 day in 250 mL HF (48.0–51.0%) to prepare the TiF_4 solution. After 1 day, the liquid was filtered using 11 m filter paper. Ammonium hydroxide (NH_4OH 28–30%) was added to the filtered liquid for complete precipitation between pH 10 and 11. The precipitates were washed repeatedly with distilled water to get rid of any undesired impurities, and dissolved in concentrated nitric acid (HNO_3, 69.5%) by heating at 80–100 °C with continuous stirring on a magnetic stirrer until a clear and homogeneous Ti^{4+} solution was achieved. In this step, a small amount of water, 10 wt% by Ti solution, was added to suppress any reprecipitation of TiO_2. To quantify the amount of Ti^{4+} in the solution, ammonium hydroxide was added to 10 mL of the solution until precipitation was complete. The precipitate was filtered and calcined along with the filter paper in an alumina crucible at 800 °C for 2 h. The weight of this calcined product was used to calculate the concentration of Ti^{4+} in solution. For Y (Yttrium)-doped TiO_2 nanopowder, $Y(NO_3)_3 \cdot 6H_2O$ was used as the starting precursor chemical for Y^{3+} source. To make 10 wt% Y_2O_3-doped nanopowder, $Y(NO_3)_3 \cdot 6H_2O$ was dissolved in 10 mL of water as a source of respective metal ions and mixed with the Ti^{4+} precursor solution.

Citric acid was then added to this Ti precursor solution with different citrate-to-nitrate ratios (C/N) of 0.1, 0.2, 0.3,

0.4, and 0.5. The solution was stirred and kept on the hot plate at ~100 °C. With the appearance of gel in the solution the temperature of the hot plate was increased to 450 °C. On complete drying, the gelatinous mass charred. The charred powder was calcined in an alumina crucible at 700 °C for 1 h to obtain the final TiO_2 nanopowder.

The sample synthesized without water showed bigger crystallite size of 20.3 nm. All synthesized TiO_2 powder had primarily the anatase phase. BET surface area analysis showed an increase in specific average surface area with increasing C/N ratio and addition of water during synthesis. The addition of water during TiO_2 synthesis increased the response of the sensors to CO at 600 °C due to reduction in particle size and increased surface area of Y-doped TiO_2 [7].

Chemical method for synthesis of Au/TiO_2 thin film

Preparation

An alcoholic (isopropanol) solution of titanium isopropoxide was mixed with a second solution, prepared by mixing dilute HCl (a few drops) and $(CH_3)_2CHOH$ [122]. The so obtained transparent sol was homogenized by magnetic stirring (200 rpm) at atmospheric condition. The formed TiO_2 particles remained in the liquid phase without any opacity for long time (1 week) and could be used to impregnate cotton fiber. After impregnation the extracted samples were placed in a preheated oven at 70 °C to remove the solvent from the fiber and then cured at 95 °C for 5 min to complete the formation of TiO_2 from the precursor. Finally, the impregnated cotton fiber samples were treated in boiling water for 3 h (post-curing). The unattached TiO_2 particles were removed from the fiber surface during the post-curing. The resultant samples were dried in a preheated oven at 40 °C. The thin film covered cotton fiber is then soaked in 0.001 M $HAuCl_4$ aqueous solution for 1 min. The sample was then dried at room temperature. To obtain gold nanoparticles, the sample with $HAuCl_4$–TiO_2 film was irradiated at 308 K (50 mW/cm^2, approx. 295–3,000 nm) for 30 min in air at atmospheric humidity.

Results of TEM shows TiO_2 particles are almost uniform in size (5–7 nm) and the gold particles are majority in the 10–12 nm range. From XRD blue shift of the absorption edge is observed on the TiO_2-covered fibers with respect to pure anatase TiO_2 is due to quantum size effects typical of small particles, which have a higher band gap with respect to that of infinite crystals. An average diameter of the TiO_2 particles is estimated about 5 nm and Au particles is estimated to be ~40 nm. Au/TiO_2 gives purple color when coated on cotton fabric [123].

Chemical method for synthesis of nano-B_2O_3/TiO_2

Preparation

Nano-TiO_2 synthesis was reported [124], which can be modified for synthesis of nano-B_2O_3/TiO_2. For this purpose, 3 g of boric acid was added into a flask containing 15 mL ethanol and 10 mL titanium tertbutoxide. The mixture was refluxed at 105 °C and during the reflux procedure ethanol, water, and HCl mixture (12.5 + 0.5 + 0.25 mL) was added. The mixture was stirred for 3 h at about 100 °C. Then, the mixture was dried for 24 h at 100 °C. The obtained solid material was ground in a ball mill for about 100 min. The powder material was taken in a porcelain crucible and heated at about 450 °C in a furnace and gray colored powder was obtained.

Nano-B_2O_3/TiO_2 composite material as a new solid phase extractor provides a simple, selective, accurate, economical, rapid, and precise method for the preconcentration and determination of cadmium [125].

Applications

Medical applications

Dental implant application

When biomaterial is implanted into the human body, it is unavoidable that blood will contact the implant surface and on contact, the implant surface could be covered with a layer of plasma proteins that mediate the next cellular responses. This leads to a better biocompatibility for the implant surface. As titanium (Ti) and its alloys have satisfactory mechanical properties, corrosion resistance, and biocompatibility, they have been widely used for orthopedic and dental implant materials. The Ti metal spontaneously forms a protective TiO_2 layer in the atmosphere. When the Ti implant is inserted into the human body, the surrounding tissues directly contact the TiO_2 layer on the implant surface. The surface characteristics of the TiO_2 layer determine the biocompatibility of Ti implant. Therefore, it is important to use appropriate surface modifications to increase the biocompatibility of the Ti implant for long-term clinical applications [126].

Polylactide nanofibers/nano-TiO_2 blends on biorecognition of anticancer drug daunorubicin

The biocompatibility and biodegradability of polylactide (PLA) polymers make them well adopted in drug delivery, tissue engineering, and temporary therapeutic applications in pharmacology and surgery. Metallic nanoparticles (e.g.,

Au or Ag) or semiconductor nanoparticles have valuable applications in electronics, optics, proteomics, and bio-analytical fields, due to their unique properties such as large surface area, pore structure, embedded effect, and size effect, unique property and high reactivity of nano-titanium dioxide (TiO_2) makes it possible to be utilized in the fields of biomedical and bioengineering.

The PLA nanofibers have been synthesized by electrospinning and the blending of nano-TiO_2–PLA nano-fibers have been utilized to remarkably enhance the performance and detection sensitivity of the bio-recognition as well as the binding affinity of anticancer drug daunorubicin to DNA.

Results of the electrochemical and atomic force microscopy (AFM) studies demonstrate that the new nano-TiO_2–PLA polymer nanocomposites could facilitate the binding of daunorubicin to DNA and remarkably enhance the detection sensitivity of the relative biomolecular recognition [127].

Applications for reducing air/water pollution

Antimicrobial nanomaterials for water disinfection and microbial control: potential applications and implications

TiO_2 can kill both Gram-negative and Gram-positive bacteria, although Gram-positive bacteria are less sensitive due to their ability to form spores. More recently, nano-sized TiO_2 was also reported to kill viruses including poliovirus 1, hepatitis B virus, Herpes simplex virus, and MS2 bacteriophage. The concentration of TiO_2 usually required to kill bacteria varies between 100 and 1,000 ppm, depending on the size of the particles and the intensity and wavelength of the light used.

The antibacterial activity of TiO_2 is related to hydroxyl free radicals and peroxide formed under UV-A irradiation via oxidative and reductive pathways, respectively. Strong absorbance of UV-A renders activation of TiO_2 under solar irradiation, significantly enhancing solar disinfection. It is found that the bacteria exposed to TiO_2 photocatalytic disinfection do not self-repair. However, bacterial death also occurred in the dark indicating that other unknown mechanisms may be involved.

TiO_2 is suitable for applications in water treatment because it is stable in water, non-toxic by ingestion and low cost and suitable for drinking water disinfection. The photoactivity in the UV-A range and the potential visible light activity when doped with metals makes TiO_2 photocatalytic disinfection especially useful in developing countries where electricity is not available. However, TiO_2-based solar disinfection is in general a very slow process due to the small fraction of UV-A in solar radiation. Therefore, success in research on metal or nitrogen doping to improve visible light absorbance of TiO_2 or UV-A activity is critical to the application of TiO_2 solar disinfection. Recently, it was demonstrated that doping TiO_2 with silver greatly improved photocatalytic bacterial inactivation by UV-A activated TiO_2 [1].

Preconcentration and separation of cadmium

Recently, determination of ultra-trace metals such as cadmium in environmental and food samples has become more serious due to increasingly lower limits imposed on trace metal content of such samples. Cadmium is one of the most dangerous trace metals in the environment of human, not only because of its high level toxicity, but also because of its wide distribution and its many important applications. The FAO/WHO Joint Expert Committee on Food Additives recommended provisional maximum tolerable daily intake of cadmium from all sources (water, food, and air) of 1.0–1.2 g/kg body mass. The maximum permissible level of cadmium in drinking water is 5.0 g/L. The direct determination of extremely low concentrations of the required trace metals by modern spectroscopic methods is still difficult due to insufficient sensitivity of the techniques and matrix interferences.

In order to overcome this problem, preliminary separation and/or preconcentration techniques for the separation of trace metals from complex matrices into a known matrix is widely used. Among the preconcentration techniques, solid phase extraction (SPE) has been used increasingly in compared with other classical methods. Numerous substances have been synthesized and used as solid phase extractor [125].

Advantages:

1. Nano-B_2O_3/TiO_2 composite material as a new solid phase extractor provides a simple, selective, accurate, economical, rapid, and precise method for the preconcentration and determination of cadmium.
2. There is no need for loading of any chelating and/or complexing agent or microorganism onto the sorbent before the preconcentration procedure to obtain quantitative recovery of cadmium ion.
3. This minimizes a possible contamination and interferences due to the reagents.
4. This feature also allows repeated use of sorbent. It was found that the recovery values of the cadmium after 100 cycles of adsorption and desorption were still quantitative.
5. Method is permitting to study in acidic medium that minimize precipitation of metal hydroxides. The main disadvantage of the proposed method is the duration time of the preconcentration step. The duration time is about 5 h for a 500 mL of sample solution [125].

Removal of 4-chlorophenol

The mesoporous TiO_2 nanoparticles was observed to be the most efficient for the degradation of 4-chlorophenol. The TiO_2 smaller particle sizes and higher surface area than the catalysts, less pore volume attributed to less reactivity for the degradation of 4-chlorophenol. Each of the operating variables applied in this study such as ultrasonic irradiation time, power density, reactor sizes, temperature of the reaction mixture, stirring effect and the H_2O/TTIP ratio was found to have a specific and major role in controlling the physicochemical properties of the TiO_2 particles investigated but no greater influence was observed with liquid phase reaction, while gaseous pollutants may show high influence on slight changes of the parameters of TiO_2 [95].

For determination of chemical oxygen demand

Chemical oxygen demand (COD) is one of the most important parameters and has been widely employed for water quality assessment, because the degradation of organic compounds requires oxygen, the quantity that they are present in a water sample can be estimated by the amount of oxygen necessary for their oxidation. The conventional method for COD determination was based on a measure of the oxygen consumed in the oxidation of organic compounds by strong oxidizing agents such as dichromate or permanganate, had several drawbacks: 2 h degradation process under high pressure and temperature, requirement of expensive (Ag_2SO_4), highly corrosive (H_2SO_4), and toxic ($HgSO_4$ and $Cr_2O_7^{2-}$) and secondary pollution is unavoidable. In addition, the sensitivity is approximately 10 mg/L, which has large error when determining the low COD values, not suitable for the determination of the tap water, spring water, and reservoir water.

Hence, the photocatalytic technology has been applied to detect the COD value, for reason of easily recombination of photogenerated electrons and holes caused the low photocatalytic efficiency of nanofilm. Hence, the composite nano-ZnO/TiO_2 was fabricated to improve the photocatalytic efficiency, additionally the control of ZnO/TiO film is more convenient than the suspension of the nanoparticles.

The photocatalytic mechanism of nano-ZnO/TiO_2 film seemed that ZnO in the nano-ZnO/TiO_2 film played an important role in the electrons transport, enhanced the separation of the photogenerated electrons and the holes, which improved the photocatalytic oxidation efficiency to the organic compounds. Under the mild conditions, a good calibration graph for COD values between 0.3 and 10 mg/L was obtained and this method was sensitive, capable of detecting as low as 0.1 mg/L COD and this method when used for real samples, it displayed some advantages, such as short analysis time, simplicity, no requirement of expensive and toxic reagents and results obtained by the method were in good agreement with the values obtained by the conventional method. Thus, it showed a promising prospect for determining the low COD values of the ground waters [128].

Nano-gold supported on TiO_2 coated glass fiber for removing toxic CO gas from air

Outstanding catalytic activities of nano-gold for oxidizing CO at low temperature, various reactions over nano-gold catalysts have been studied. These include CO oxidation, preferential oxidation of CO in the presence of excess hydrogen (PROX), water gas shift reaction (WGSR), hydrogenation, and oxidation. However, in most investigations, the nano-gold particles (some in the form of gold nanotubes) are supported on metal oxide powders, such as TiO_2, Fe_2O_3, Al_2O_3 and $MgAl_2O_4$, or on porous materials, such as zeolite, on the other hand, the powder form of these catalysts may limit their application, because the drop in pressure becomes an important problem when the packing density of the powder is too high. Hence, nano-gold was prepared on glass fiber is expected to have various applications, one of which is as a packing material in safety gas masks for removing toxic CO gas from air because nano-gold catalysts have advantages over other catalysts for removing CO, including higher reaction activity at room temperature and higher moisture resistant.

The catalytic activity of nano-gold supported on TiO_2-coated glass fibers depends on the TiO_2 crystal size. Au/TiO_2-glass fiber catalysts can continuously convert CO to CO_2 for more than 15 min, meeting the European standard [129].

Application of nano-TiO_2 toward polluted water treatment combined with electro-photochemical method

With the rapid development of industry and fast increase of population density in city, a variety of poisonous and harmful substances, especially organic pollutants, were discharged into natural waters without appropriate treatment, which has caused serious pollution. Up to now, great attention has been paid to water pollution and its treatment, photocatalysis because it can completely degrade the organic pollutants into harmless inorganic substances (such as CO_2, H_2O, etc.) under moderate conditions, and would not bring with any serious secondary pollution.

Nano-TiO_2 is one of the suitable semiconductors for photocatalyst but its properties, not only the photoefficiency or activity but also the photo response are not sufficient, for

the moment the high recombination ratio of photoinduced hole–electron pairs also reduces its catalytic efficiency. Therefore, various modifications have been performed on nano-TiO_2 to promote its catalytic ability and develop new photocatalytic functions [130].

Photocatalytic oxidation of VOCs using nano-TiO_2 photocatalyst

Indoor air pollution is becoming a serious problem recently. Pollutants in indoor air such as volatile organic compounds (VOCs), NO*x*, and SO_2 can cause adverse health impacts on occupants. VOCs are the main components of the indoor air pollutants, which are from indoor furnishing, tobacco smoke, vehicular emissions, and the use of liquefied petroleum gas. Conventionally, VOCs pollutants are removed by air purifiers that employ filters to remove particulate matters or use sorption materials (e.g., granular-activated carbon) to adsorb the pollutants. Improper maintenance of these purifiers may even become a source of pollutant. The photocatalytic process is emerging as a promising alternative technology for the degradation of VOCs. The thin film nano-TiO_2/UV process is an advanced oxidation process. TiO_2 is superior to other photocatalysts because of its interesting characteristics:

(a) It is low cost, safe, and very stable showing high photocatalytic efficiency;
(b) It promotes ambient temperature oxidation of the major classes of indoor air pollutants;
(c) Complete degradation of a broad range of pollutants can be achieved under certain operating conditions;
(d) No chemical additives are needed.

It is known that the thin film nano-TiO_2 photocatalytic degradation efficiency of VOCs can be potentially limited by several parameters.

(a) The degradation efficiency may be very low inside a thick catalyst due to the UV light intensity attenuation by the catalyst.
(b) The VOCs molecules diffusion in the catalyst can be very slow so that there are not enough molecules available for degradation inside the catalyst [131].

Applications in sensors

Quartz crystal microbalance sensor and its thermal behavior studies

Gas sensors based on conducting polymers are particularly attractive as these compounds can be modified chemically to exhibit a high sensitivity to a range of gases and vapors, and have the potential for room operation. Conducting polymers have good mechanical properties, which allow a facile fabrication of sensors. A simple and repeatable polyaniline (PANI)–TiO_2 composite-based gas sensor for detection of trimethylamine at room temperature is developed by a quartz crystal microbalance (QCM) method.

The sensor exhibited a good linear response to trimethylamine, had a good selectivity against ethanol, formaldehyde, and acetaldehyde. Response time of the sensor to trimethylamine is <300 s, and the response can be recovered by N_2 purgation easily.

The FTIR spectra and QCM results of these two materials indicated that storing the PANI would absorb some small molecules in air, which could reduce its trimethylamine sensitivity.

The sensitivity variation due to temperature change under 100 °C could be avoided by doping PANI with TiO_2. PANI–TiO_2 nanocomposite had better thermal tolerance than PANI without TiO_2 and the feasibility of PANI–TiO_2 nanocomposite as a trimethylamine gas-sensitive membrane for QCM sensors in specific practical applications.

However, the sensing properties of PANI–TiO_2 nanocomposite, including sensitivity, response time, and selectivity, etc., are not good enough. We will do further research to improve its gas-sensing properties and apply it practically [132].

Aluminum-doped TiO_2 nanopowders for gas sensors

Transition metal oxides are the most widely used ceramics for gas sensor applications. A change in their electrical conductivity due to the presence of a target gas is used for sensing measurement. Among different transition metal oxides, SnO_2-based sensors are the most widely used. As gas-sensitive resistors, these sensors show good sensitivity and selectivity below 250 °C. However, at temperatures >250 °C, SnO_2-based sensors show poor sensitivity due to lack of stability. It has been reported that titanium dioxide (TiO_2)-based gas sensors show good sensitivity and stability in adverse environments and have the potential to become the material of choice for high temperature gas sensors.

It has been shown that sensitivity of TiO_2 sensors can be improved by the addition of dopants such as Nb, Cr, Sn, Pt, Zn, Al, La, and Y. The most important effects of dopant addition in TiO_2 are increasing the conductivity, slowing down anatase-to-rutile transformation, and reducing grain growth. Among those dopants, Al-doping in TiO_2 shows retardation of phase transformation from anatase to rutile by stabilizing the surface state of TiO_2 particles and also inhibits grain growth. It has been reported that the conductivity of the Al-doped TiO_2 is higher than that of pure TiO_2, also enhances sensitivity and selectivity toward certain gasses, also been shown to have higher sensitivity

to humidity in thick and thin films. With dopant addition, higher crystallinity was also needed to improve sensitivity of these gas sensors [133].

Special applications

Self-cleaning of modified cotton textiles by TiO_2 at low temperatures under daylight irradiation

Acrylic emulsions of TiO_2 have been coated on textiles with the purpose of inducing self-cleaning effects under daylight irradiation, but the coating showed some degradation after being exposed to the action of daylight. The commercial potential of the TiO_2 semiconductor on cotton textiles prepared at relatively low temperatures for self-cleaning purposes, aims at the discoloration of organic materials including dyes, pigments, and grease on the modified cotton textile loaded with TiO_2. The use of TiO_2 loaded flexible substrates will possibly allow their application during the photodegradation of micelles, oils, solvents, sooth, aromatic, and aliphatic hydrocarbons under daylight.

The fabric is coated with a thin layer of titanium dioxide nanoparticles. When this semi-conductive layer is exposed to light, photons with energy equal to or greater than the band gap of the titanium dioxide excite electrons up to the conduction band. The excited electrons within the crystal structure react with oxygen atoms in the air, creating free-radical oxygen. These oxygen atoms are powerful oxidizing agents, which can break down most carbon-based compounds through oxidation–reduction reactions. In these reactions, the organic compounds (i.e., dirt, pollutants, and microorganisms) are broken down into substances such as carbon dioxide and water. Since the titanium dioxide only acts as a catalyst to the reactions, it is never used up. This allows the coating to continue breaking down stains over and over [121] (Fig. 5).

On the electrode of dye-sensitized solar cells

Dye-sensitized solar cells (DSSCs) based on nano-crystalline TiO_2 electrodes are low cost alternative to conventional inorganic photovoltaic devices. The function of such devices is based upon the injection of an electron from a photoexcited state of the sensitizer dye into the conduction band of the semiconductor. These dyes show an efficient sensitive effect due to their strong absorption in the visible region.

TCPP/TiO_2 are shifted to higher binding energies, indicate that the effects of nano-TiO_2 particles addition in the electrode of dye-sensitized solar cell can improve the absorption of visible light and increase electrons transferred from TCPP to the conduction band of TiO_2, resulting in the enhancement of efficiency for dye-sensitized solar cell [134].

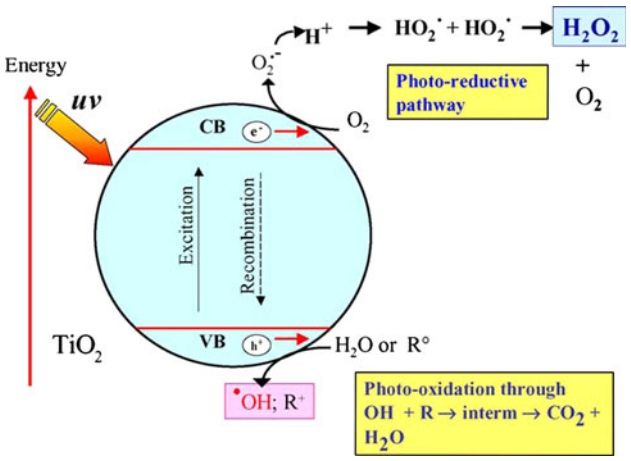

Fig. 5 Classical scheme for the production of highly oxidative species by TiO_2 under light irradiation with wavelengths <400 nm

Smart corrosion resistant coatings

PANI is conducting polymers have various applications such as sensors, transparent conductor, electro static discharge (ESD) and electro magnetic interference (EMI) protection, electrochromic displays, etc. and recently as an effective material for corrosion protection. A number of other authors have reported the use of PANI with other additives in corrosion protection but mostly these are in macroparticulate form.

In corrosion protection by organic coatings, there can be barrier effect and internal sacrificial electrode formation, which give protection to the underlying substrate. The barrier properties can be enhanced if appropriate fillers in the coatings are used and nanoparticulate fillers give much better barrier properties even at low concentrations than conventional micron size additives.

Titanium dioxide (rutile or anatase) is commonly used as a pigment material for paints, it is thought worthwhile to use nanoparticulate TiO_2 as a metal oxide additive in the composite which can give better dispersion of the formulation, barrier properties in the coatings, self-healing effect giving advantage in anticorrosion behavior.

Hence, if the main resin is damaged, the additives give a healing effect and prevent catastrophic failure, these coatings have good gloss and shiny surface, which is not easily obtained in conventional coating, prepared with commercial micron size particle additives. Such systems can be used as a primer coat or even as a single coating on steel, where color is not a very important criterion [135].

Effect of nano-TiO_2 long-term exposure

With increased application of TiO_2 nanoproducts (nano-TiO_2) on the other hand comes the inevitable possibility of

effects on the health of humans exposed to these products. A number of studies indicate that nano-TiO_2 exhibit concerned cytotoxicity in different cultured cell models and nano-TiO_2 catalyzes the formation of superoxide, H_2O_2, and hydroxyl radicals resulting in cytotoxicity and genotoxicity in different mammalian cells but the controversial cellular responses to different doses of nano-TiO_2 are also observed. Ranging from 5 to 200 μg/ml for 12–72 h exposure, nano-TiO_2 displayed significant non-cytotoxic and non-genotoxic effect to different cultured cells.

Results demonstrate that long-term exposure to nano-TiO_2 disturbs cell cycle development and duplicated genome segregation, leading to chromosomal instability and cell transformation [136].

References

1. Li Q, Mahendra S, Lyon DY, Brunet L, Liga MV, Li D, Alvarez PJJ (2008) Water Res 42:4591
2. Beydoun D, Amal R, Low G, Mcevoy S (1999) J Nanoparticle Res 1:439
3. Blake DM, Maness PC, Huang Z, Wolfrum EJ, Huang J, Jacoby WA (1999) Sep Purif Methods 28:1
4. Sthathatos E, Tsiourvas D, Lianos P (1999) J Colloids Surf A 149:49
5. Comparelli R, Fanizza E, Curri ML, Cozzoli PD, Mascolo G, Passino R, Agostiano A (2005) Appl Catal B 55:81
6. Vijay M, Selvarajan V, Sreekumar KP, Yu J, Liu S, Ananthapadmanabhan PV (2009) Sol Energy Mater Sol Cells 93:1540
7. Seeley Z, Choi YJ, Bose S (2009) Sens Actuators B 140:98
8. Gianluca L, Bono A, Krishnaiah JG, Collin D (2008) J Hazard Mater 157(2–3):209
9. Meacock G, Taylor KDA, Knowles M, Himonides A (1997) J Sci Food Agric 73(2):221
10. Yu H-F, Zhang Z-W, Hu F-C (2008) J Alloys Compd 465:484
11. Carp O, Huisman CL, Reller A (2004) Progr Solid State Chem 32:33
12. Gaya UI, Abdullah AH (2008) J Photochem Photobiol C 9:1
13. Patil KC, Hegde MS, Rattan T, Aruna ST (2008) Chemistry of nanocrystalline materials: combustion synthesis, properties and applications. World Scientific, London, pp 179–209
14. Gerven TV, Mul G, Moulijn J, Stankiewicz A (2007) Chem Eng Proc 46:781
15. Li J-G, Kamiyama H, Wang X-H, Moriyoshi Y, Ishigaki T (2006) J Eur Ceram Soc 26:423
16. Page K, Palgrave RG, Parkin IP, Wilson M, Savin SLP, Chadwick AV (2007) J Mater Chem 17(1):95
17. Reddy MP, Venugopal A, Subrahmanyam M (2007) Water Res 41:379
18. Rehman S, Ullah R, Butt AM, Gohar ND (2009) J Hazard Mater 170:560
19. Nakamura I, Negishi N, Kutsuna S, Ihara T, Sugihara S, Takeuch K (2000) J Mol Catal A 161:205
20. Ihara T, Miyoshi M, Iriyama Y, Matsumoto O, Sugihara S (2003) Appl Catal B 42:403
21. Ghorai TK, Dhak D, Biswas SK, Dalai S, Pramanik P (2007) J Mol Catal A 273:224
22. Babelon P, Dequidt AS, Mostefa-Sba H, Bourgeois S, Sibillot P, Sacilotti M (1998) Thin Solid Films 322:63
23. Kim B-H, Lee J-Y, Choa Y-H, Higuchi M, Mizutani N (2004) Mater Sci Eng B 107:289
24. Okuyama K, Shimada M, Fujimoto T, Maekawa T, Nakaso K, Seto T (1998) J Aerosol Sci 29(1):S907
25. Gu D-E, Yang B-C, Hu Y-D (2008) Catal Commun 9:1472
26. Su C, Hong BY, Tseng CM (2004) Catal Today 96:119
27. Sun J, Wang X, Sun J, Sun R, Sun S, Qiao L (2006) J Mol Catal A 260:241
28. Rengaraj S, Li XZ, Tanner PA, Pan ZF, Pang GKH (2006) J Mol Catal A 247:36
29. Yu H, Zheng X, Yin Z, Tao F, Fang B, Hou K (2007) Chin J Chem Eng 15(6):802
30. Liu S, Yang J-H, Choy J-H (2006) J Photochem Photobiol A 179:75
31. Ding X, An T, Li G, Zhang S, Chen J, Yuan J, Zhao H, Chen H, Sheng G, Fu J (2008) J Colloid Interface Sci 320(2):501
32. Li Y, Peng S, Jiang F, Lu G, Li S (2007) J Serb Chem Soc 72(4):393
33. Liao DL, Badour CA, Liao BQ (2008) J Photochem Photobiol A 194:11
34. Rengaraj S, Li XZ (2006) Int J Environ Pollut 27(1/2/3):20
35. Xu A-W, Gao Y, Liu H-Q (2002) J Catal 207:151
36. Liu G, Zhang X, Xu Y, Niu X, Zheng L, Ding X (2005) Chemosphere 59:1367
37. Xin B, Wang P, Ding D, Liu J, Ren Z, Fu H (2008) Appl Surf Sci 25(4):2569
38. Bu S, Jin Z, Liu X, Yin T, Cheng Z (2006) J Mater Sci 41(7):2067. doi:10.1007/s10853-006-8000-y
39. Colmenares JC, Aramendia MA, Marinas A, Marinas JM, Urbano FJ (2006) Appl Catal A 306:120
40. Campostrini R, Ischia M, Palmisano L (2003) J Therm Anal Calorim 71(3):997
41. Campostrini R, Ischia M, Palmisano L (2003) J Therm Anal Calorim 71(3):1011
42. Campostrini R, Ischia M, Palmisano L (2004) J Therm Anal Calorim 75(3):13
43. Campostrini R, Ischia M, Palmisano L (2004) J Therm Anal Calorim 75(1):25
44. Crisan M, Braileanu A, Raileanu M, Zaharescu M, Crisan D, Dragan N, Anastasescu M, Ianculescu A, Nitoi I, Marinescu VE, Hodorogea SM (2008) J Non-Cryst Solids 354:705
45. Fan X, Chen X, Zhu S, Li Z, Yu T, Ye J, Zou Z (2008) J Mol Catal A 284:155
46. Gombac V, Rogatis LD, Gasparotto A, Vicario G, Montini T, Barreca D, Balducci G, Fornasiero P, Tondello E, Graziani M (2007) Chem Phys 339:111
47. Li XZ, Li FB, Yang CL, Ge WK (2001) J Photochem Photobiol A 141:209
48. Li Y, White TJ, Lim SH (2004) J Solid State Chem 177(4–5):1372
49. Peng A, Xie E, Jia C, Jiang R, Lin H (2005) Mater Lett 59(29–30):3866
50. Saif M, Abdel-Mottaleb MSA (2007) Inorg Chim Acta 360:2863
51. Shi J-W, Zheng J-T, Hu Y, Zhao Y-C (2007) Mater Chem Phys 106:247
52. Sivakumar S, Krishna PP, Makundan P, Warrier KGK (2002) Mater Lett 57(2):330
53. Srinivasan SS, Wade SJ, Stefanakos EK, Goswami Y (2006) J Alloys Compd 424:322
54. Stir M, Nicula R, Burkel E (2006) J Eur Ceram Soc 26:1547
55. Watson SS, Beydoun D, Scott JA, Amal R (2003) Chem Eng J 95(1):213
56. Wilke K, Breuer HD (1999) J Photochem Photobiol A 121:49
57. Xu W, Hu W, Li M, Wen C (2006) Mater Lett 60(13–14):1575
58. Yang Y, Li X-J, Chen J-T, Wang L-Y (2004) J Photochem Photobiol A 163:517

59. Zaleska A, Sobczak JW, Grabowska E (2008) J Hupka Appl Catal B 78:92
60. Zhang X, Liu Q (2008) Mater Lett 62:2589
61. Peng F, Cai L, Huang L, Yu H, Wang H (2008) J Phys Chem Solids 69(7):1657
62. Peng F, Cai L, Huang L, Yu H, Wang H (2008) J Solid State Chem 181:130
63. Feng X, Wang Q, Wang G, Qiu F (2006) Chin J Catal 27(3):195
64. Wang F, Shi Z, Gong F, Jiu J, Adachi M (2007) Chin J Chem Eng 15(5):754
65. Zhiyu W, Haifeng C, Peisong T, Weiping M, Fuan Z, Guodong Q, Xianping F (2006) Colloids Surf A 289:207
66. Zhu J, Deng Z, Chen F, Zhang J, Chen H, Anpo M, Huang J, Zhang L (2006) Appl Catal B 62:329
67. Bettinelli M, Dallacasa V, Falcomer D, Fornasiero P, Gombac V, Montini T, Romano L, Speghini A (2007) J Hazard Mater 146:529
68. Liu C, Tanga X, Moa C, Qiang Z (2008) J Solid State Chem 181(4):913
69. Tanaka K, Hisanaga T, Harada K (1989) J Photochem Photobiol A 48:155
70. Horikawa T, Katoh M, Tomida T (2008) Microporous Mesoporous Mater 110:397
71. Chen L-C, Huang C-M, Tsai F-R (2007) J Mol Catal A 265: 133
72. Huang M, Xu C, Wu Z, Huang Y, Lin J, Wu J (2008) Dyes Pigm 77:327
73. Sun J, Qiao L, Sun S, Wang G (2008) J Hazard Mater 155:312
74. Lee A-C, Lin R-H, Yang C-Y, Lin M-H, Wang W-Y (2007) Mater Chem Phys 109(2–3):275
75. Jeon MS, Yoon WS, Joo H, Lee TK, Lee H (2000) Appl Surf Sci 165:209
76. Oh SM, Ishigaki T (2004) Thin Solid Films 457:186
77. Kakati M, Bora B, Sarma S, Sripathi T, Deshpande U, Dubey A, Ghosh G, Das AK (2008) Vacuum 82:833
78. Kitazawa S (2004) Jpn J Appl Phys 43:6335
79. Ohshima T, Nakashima S, Ueda T, Kawasaki H, Suda Y, Ebihara K (2006) Thin Solid Films 106:506
80. Thareja RK, Sharma AK (2006) Laser Part Beams 24:311
81. Belkind A, Zhu W, Lopez J, Becker K (2006) Plasma Sources Sci Technol 15:S17
82. Matsushima Y, Yamazaki T, Maeda K, Noma T, Suzuki T (2006) J Am Ceram Soc 89(3):799
83. Nakamura M, Kato S, Aoki T, Sirghi L, Hatanaka Y (2001) Thin Solid Films 401:138
84. Borras A, Cotrino J, Gonzalez-Elipe AR (2007) J Electrochem Soc 154:152
85. Li C-J, Yang G-J, Wang Z (2003) Mater Lett 57:2130
86. Jang HD, Kim S-K (2001) Mater Res Bull 36:627
87. Tung WS, Daoud WA (2008) J Colloid Interface Sci 326:283
88. Körösi L, Dékány I (2006) Colloids Surf A 280:146
89. Suslick KS (1990) Science 247:1439
90. Koda S, Tanaka K, Sakamoto H, Matsuoka T, Nomura H (2004) J Phys Chem A 108:11609
91. Ramakrishna G, Singh AK, Palit DP, Ghosh HN (2004) J Phys Chem B 108:4775
92. Neppolian B, Jung H, Choi H, Lee JH, Kang JW (2002) Water Res 36:4699
93. Neppolian B, Park JS, Choi H (2004) Ultrason Sonochem 11:273
94. Koda S, Kimura T, Kondo T, Mitome H (2003) Ultrason Sonochem 10(3):149
95. Neppolian B, Wang Q, Jung H, Choi H (2008) Ultrason Sonochem 15(4):649
96. Hong S-S, Lee MS, Hwang H-S, Lim K-T, Park S-S, Ju C-S, Lee G-D (2003) Sol Energy Mater Sol Cells 80(3):273
97. Mejiá MI, Mariń JM, Restrepo G, Pulgariń C, Mielczarski E, Mielczarski J, Arroyo Y, Lavanchy J-C, Kiwi J (2009) Appl Catal B 91:481
98. Payakgul W, Mekasuwandumrong O, Pavarajarn V, Praserthdam P (2005) Ceram Int 31:391
99. Supphasrirongjaroen P, Praserthdam P, Panpranot J, Na-Ranong D, Mekasuwandumrong O (2008) Chem Eng J 138:622
100. Kang M, Lee S-Y, Chung C-H, Cho SM, Han GY, Kim B-W, Yoon KJ (2001) J Photochem Photobiol A 144:185
101. Kang M, Ko Y-R, Jeon M-K, Lee S-C, Choung S-J, Park J-Y, Sung K, Choi S-H (2005) J Photochem Photobiol A 173:128
102. Ku Y, Ma C, Shen Y (2001) Appl Catal B 34:181
103. Dong Y, Bai Z, Liu R, Zhu T (2007) Catal Today 126:320
104. Leea J-E, Ohb S-M, Parka D-W (2004) Thin Solid Films 457:230
105. Kakati M, Bora B, Deshpande UP, Phase DM, Sathe V, Lalla NP, Shripathi T, Sarma S, Joshi NK, Das AK (2009) Thin Solid Films 518(1/2):84
106. Liu B, Torimoto T, Yoneyama H (1998) J Photochem Photobiol A 115:227
107. Kasuga T, Hiramatsu M, Hirano M, Hosono A, Oyamada K (1997) J Mater Res 12(3):607
108. Zhu Y, Ding C (2000) J Eur Ceram Soc 20(2):127
109. Matin N, Rousselot C, Rondot D, Palmino F, Mercier R (1997) Thin Solid Films 300(1/2):113
110. Mandl S, Thorwarth G, Schreck M, Stritzker B, Rauschenbach B (2000) Surf Coat Technol 125(1–3):84
111. Li Y-L, Ishigaki T (2002) Thin Solid Films 407(1–2):79
112. Padmanabhan PVA, Sreekumar KP, Thiyagarajan TK, Satpute RU, Bhanumurthy K, Sengupta P, Dey GK, Warrier KGK (2006) Vaccum 80(11–12):1252
113. Wei D, Zhou Y, Jia D, Wang Y (2008) Appl Surf Sci 254:1775
114. Zhu YC, Huang MH, Xia JY, Ding CX (1997) J Korean Vac Soc 6(S1):23
115. Powder Diffraction File, No. 18-1402 (1983) Inorganic volume, no. PDIS-22IRB, published by the JCPDS International Center for Diffraction Data, 1601 Park Lane, Swarthmore, Pennsylvania, 19081 USA
116. Zhu YC, Ding CX (1999) Nanostrut Mater 11(3):319
117. Kosmulski M, Mczkaa E, Januszc W, Rosenholmb JB (2002) Adv Colloid Interface Sci 250(1):99
118. Perego C, Revel R, Durupthy O, Cassaignon S, Jolivet JP (2010) Solid State Sci 12(6):989
119. Imagawa H, Tanaka T, Takahashi N, Matsunaga S, Suda A, Shinjoh H (2007) J Catal 251:315
120. Pechini M (1967) U.S. Patent #3,330,697
121. Choi Y, Seeley Z, Bandyopadhyay A, Bose S, Akbar S (2007) Sens Actuators B 124:111
122. Uddin MJ, Cesano F, Bonino F, Bordiga S, Spoto G, Scarano D, Zecchina A (2007) J Photochem Photobiol A 189(2):286
123. Uddin MJ, Cesano F, Scarano D, Bonino F, Agostini G, Spoto G, Bordiga S, Zecchina A (2008) J Photochem Photobiol A 199(1):64
124. Liu Y, Liang P, Guo L (2005) Talanta 68:25
125. Kalfa OM, ınkaya OY, Turker AR (2009) J Hazard Mater 166:455
126. Yang WE, Hsu ML, Lin MC, Chen ZH, Chen LK, Huang HH (2009) J Alloys Compd 479:642
127. Song M, Pan C, Chen C, Li J, Wang X, Gu Z (2008) Appl Surf Sci 255:610
128. Zhang Z, Yuan Y, Fang Y, Liang L, Ding H, Jin L (2007) Talanta 73(3):523
129. Kuo CN, Chen HF, Lin JN, Wan BZ (2007) Catal Today 122:270
130. Chen J, Liu M, Zhang L, Zhang J, Jin L (2003) Water Res 37:3815

131. Yu H, Zhang K, Rossi C (2007) J Photochem Photobiol A 188:65
132. Zheng J, Li G, Ma X, Wang Y, Wu G, Cheng Y (2008) Sens Actuators B 133:374
133. Bozzi A, Yuranova T, Guasaquillo LD, Kiwi J (2005) J Photochem Photobiol A 174:156
134. Meen TH, Water W, Chen WR, Chao SM, Ji LW, Huang CJ (2009) J Phys Chem Solids 70:472
135. Radhakrishnan S, Siju CR, Mahanta D, Patil S, Madras G (2009) Electrochim Acta 54:1249
136. Huang S, Chueh PJ, Lin YW, Shih TS, Chuang SM (2009) Toxicol Appl Pharmacol 241(2):182